Journal of Multidisciplinary Engineering Science and Technology (JMEST)
ISSN: 3159-0040
Vol. 2 Issue 11, November - 2015

Design and Analysis of a System for Precise Speed Control of a DC Motor

Prof. Kamen M. Yanev
Professor, Department of Electrical Engineering, Faculty of Engineering and Technology
University of Botswana
Gaborone, Botswana
yanevkm@yahoo.com; yanevkm@mopipi.ub.bw

***Abstract*—The contribution of this research is in suggesting a useful method for precise speed control of a dc motor. The paper describes an application, where the armature of a dc motor is connected as one of the ratio arms of a Wheatstone bridge, now becoming an active dc bridge. The bridge is originally balanced for static armature conditions. Under running conditions of the dc motor, the bridge becomes unbalanced and its output voltage is continuously compared with a preset reference quantity. The electronic comparator can be designed as a nonlinear on-off element with hysteresis, while the complete control system is a combination of a linear and a nonlinear part. The system is analyzed for stability with the aid of the advanced D-partitioning and the Goldfarb stability criterion.**

Keywords— Speed control; torque; nonlinear; stability; advanced D-partitioning; describing function analisis;

I. INTRODUCTION

A useful technique is proposed to design precise speed control of a dc motor. Maintaining very accurately a constant speed of a dc motor, subjected to a variable torque, is an important task in many industrial applications. Control system keeping a constant motor speed should incorporate some type of a speed-to-voltage converter in its feedback loop. Considering different methods of obtaining a signal proportional to the speed of the motor, an alternative solution is suggested, introducing an active dc bridge (ADCB), where the armature circuit of a separately excited dc motor is connected as one of the ratio arms of a Wheatstone bridge.

The advantage of the ADCB is that it is not bringing any additional time constants and its output voltage depends directly on the armature emf, therefore on the speed of the dc motor. Further, the accuracy of this method is independent of the resistive bridge components. When applying an ADCB in a control system, it is essential to analyze its dynamics and derive its transfer function. Data obtained by the operation of the ADCB and the control system under operation, prove a successful solution of the speed-voltage conversion used for accurate speed control of dc motors.

II. STRUCTURE AND ANALYSIS OF THE ADCB

The armature circuit of a separately excited dc motor is connected as one of the ratio arms of a Wheatstone bridge, shown in Figure 1. The bridge, connected to a dc supply voltage *V*, is originally balanced at idle armature conditions. Then only the armature resistance R_a participates in the bridge ratio arm *bc,* since the dc motor does not induce armature emf *E* at these circumstances.

It is essential to limit the current in the branches *ad* and *ac*, therefore the resistors R_1 and R_2 must be of high value. They are used to balance the bridge at standstill motor conditions. The resistance R_3 is equivalent in value with the rate of the armature resistance R_a. Also, it is assumed that the internal resistance of the supply voltage is equal to zero.

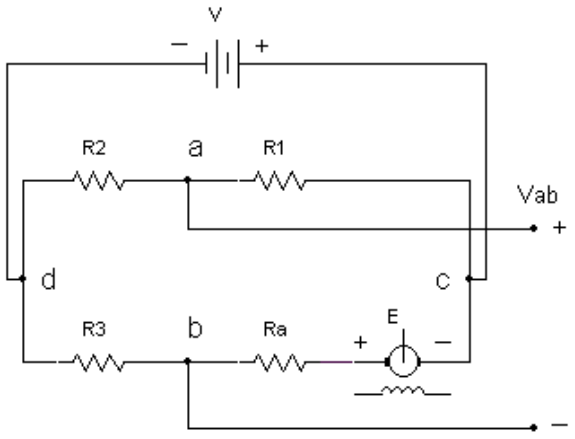

Figure 1: Active dc Bridge (ADCB)

At running conditions of the dc motor, an armature emf *E* is induced and the Wheatstone bridge becomes unbalanced.

By deriving the transfer function of the ADCB, analyzing its circuit diagram and taking into account its dynamics, it can be proved that the bridge output voltage V_{ab} depends directly on the induced armature emf *E* and hence on the motor speed *n*.

The output voltage of the bridge can be presented as follows:

$$V_{ab} = V_{cb} - V_{ca} \quad (1)$$

where

$$V_{cb} = E + I_a R_a = E + \frac{V - E}{R_3 + R_a} R_a = \\ = E\left(1 - \frac{R_a}{R_3 + R_a}\right) + V\frac{R_a}{R_3 + R_a} = \\ = E\frac{R_3}{R_3 + R_a} + V\frac{R_a}{R_3 + R_a} \quad (2)$$

I_a is the armature current

$$V_{ca} = V\frac{R_1}{R_1 + R_2} \quad (3)$$

After substituting Equations (2) and (3) in (1):

$$V_{ab} = E\frac{R_3}{R_3 + R_a} + V\frac{R_a}{R_3 + R_a} - V\frac{R_1}{R_1 + R_2} \quad (4)$$

The transfer function of an armature-controlled dc motor [2] is considered as well

$$G(s) = \frac{\omega(s)}{V_{cb}(s)} = \frac{K}{\tau_a T_m s^2 + \tau_m s + 1} \quad (5)$$

where $\omega = \frac{2\pi}{60} n\,\omega$ is the speed of the motor in rad/s

K is the gain of the motor

τ_a is the armature time constant of the motor

τ_m is the electromechanical time constant of the motor

s is the Laplace operator

The following constants can be introduced:

$$K_1 = \frac{R_1}{R_1 + R_2}, K_2 = \frac{R_a}{R_a + R_3}, K_3 = K,$$

$$K_4 = \frac{60}{2\pi}, \; K_5 = c_e\phi, \; K_6 = \frac{R_3}{R_3 + R_a},$$

where c_e = Constant

ϕ is the flux of the exciting coil

Considering Equations (4) and (5), a block diagram of the ADCB is developed. The signal flow in the diagram is based on the principle of operation of the ADCB, as shown in Figure 2. The ADCB transfer function can be determined as the ratio of its output and input signals

$$G_{ADCB}(s) = \frac{V_{ab}(s)}{V(s)} \quad (6)$$

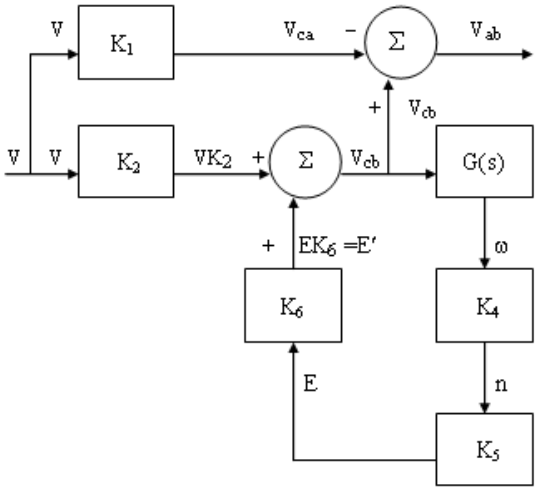

Figure 2: Block diagram of an ADCB

The positive feedback loop of the block diagram in Figure 2 can be used to derive the following equivalent transfer function:

$$G_{eq}(s) = K_4 K_5 K_6 G(s) = \frac{K_3 K_4 K_5 K_6}{\tau_a \tau_m s^2 + \tau_m s + 1} \quad (7)$$

By implementing some of the Block Diagram Algebra rules [1], the original system is simplified in achieving successive reduction of the blocks.

The diagram in Figure 3(a) is showing reduction of blocks of the original system by combining cascaded elements in its feedback loop.

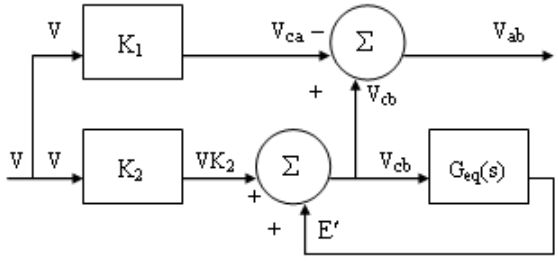

Figure 3(a): Reduction of the ADCB block diagram (Step 1)

Figure 3(b) represents the movement of a pickoff point behind a block.

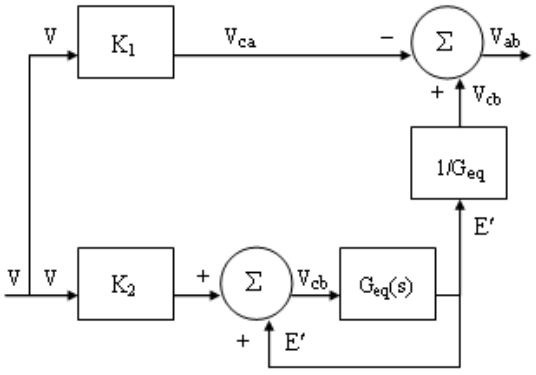

Figure 3(b): Reduction of the ADCB block diagram (Step 2)

In Figure 3(c) the positive feedback loop is eliminated.

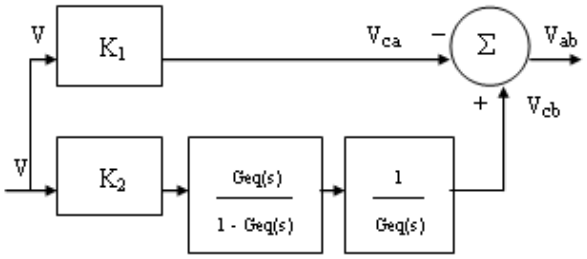

Figure 3(c): Reduction of the ADCB block diagram (Step 3)

Next, in Figure 3(d), a combination of cascaded blocks is represented.

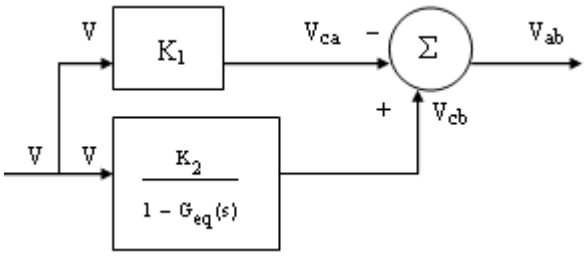

Figure 3(d): Reduction of the ADCB block diagram (Step 4)

Finally, in Figure 3(e), two parallel branches are combined to determine the ADCB transfer function as follows

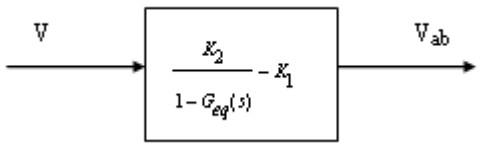

Figure 3(e): Reduction of the ADCB block diagram (Step 5)

$$G_{ADCB}(s)=\frac{V_{ab}(s)}{V(s)}=\frac{K_2}{1-G_{eq}(s)}-K_1 \qquad (8)$$

Substituting Equation (7) in (8) results in

$$G_{ADCB}(s)=\frac{(K_2-K_1)(\tau_a\tau_m s^2+\tau_m s+1)+K_1K_3K_4K_5K_6}{\tau_a\tau_m s^2+\tau_m s+1-K_3K_4K_5K_6} \qquad (9)$$

Since $K_2-K_1=R_2R_a-R_1R_3=0$ for a balanced ADCB, finally its transfer function can be presented as

$$G_{ADCB}(s)=\frac{V_{ab}}{V}=\frac{K_1K_3K_4K_5K_6}{\tau_a\tau_m s^2+\tau_m s+1-K_3K_4K_5K_6} \qquad (10)$$

Equation (10) shows that the ADCB can be considered as a second order model, for this reason it is expected that its transient response to a step-input signal is a damped oscillation [2], [3]. Also, since both Equations (5) and (10) are of second order, a comparison between them proves that the speed of the dc motor *n*, rpm is directly proportional to the output voltage of the ADCB V_{ab}. Considering the relationship:

$$G(s)=\frac{\omega(s)}{V_{cb}(s)}\propto G_{AWB}(s)=\frac{V_{ab}(s)}{V(s)} \qquad (11)$$

It follows that

$$n(s)=\frac{60}{2\pi}\omega(s)\propto V_{ab}(s) \qquad (12)$$

III. Speed Control System Employing an ADCB

The ACDB is involved in a closed-loop control system. Its block diagram is shown in Figure 4. The objective of the control system is to maintain constant speed of the dc motor. There are two external disturbances to the system: variations of the load torque T_L and variations of the supply ac voltage *V*. The control system is a sophisticated combination of a linear and a nonlinear part. Three possible input control signals are considered: V_r (setting the driving torque T_D), *r* (setting the firing angle α) and T_L (the load torque applied to the dc motor). The system is described in a way that for a set voltage V_r the output signal is the motor's speed *n*.

The supply ac line voltage *V* is applied to a thyristor Bridge Rectifier (BR). The output voltage of the BR V_{cd} is applied to a Wheatstone bridge (WB). The armature of the dc motor (M) is connected as one of the arms of the WB. The interaction of the M and the WB is a unique arrangement and a new technical solution as already described as (ADCB).

The output voltage of the ADCB V_{fb} is an important feedback signal and depends only on the motor's armature emf $E = V_{bc}$ [4]. Variable load torque T_L, applied to the motor, or the supply ac line *V* voltage does not affect its speed of the dc motor because of the tight closed-loop control.

The feedback voltage V_{fb} is applied to a Reference and Comparison Unit (RCU). There it is compared with a reference voltage V_r. The RCU is a comparator, operating as a nonlinear ON-OFF element with hysteresis [5], [6]. Its output signal *n* controls the variable-phase pulse generator (VPPG).

The VPPG consists of a current generator (CG) and a threshold unit (TU). The output voltage of the CG V_c is applied to the TU in this way controlling the thyristor-firing delay angles α of the BR [5], [6].

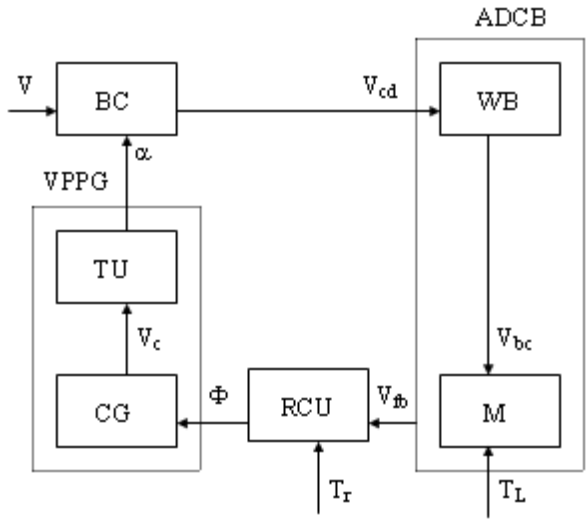

Figure 4: Block diagram of the closed-loop speed control system

IV. Control System Operation

The electronic circuit diagram of the speed control system is shown in Figure 5. The principle of operation of is described following the sequence of the control signals [5], [6].

The ac line voltage is applied to the BC via a filter (C_1, L_1, L_2). This voltage is also applied via two step-down centre-tapped transformers (Tr_2, Tr_3) to rectifiers providing supply to the RCU and the VPPG. The bridge converter consists of two thyristors Th_1, Th_2 and two diodes D_1, D_2. Its output controlled dc voltage is applied to the *cd* diagonal of the ADCB. To balance the ADCB, operating as an Active Wheatstone Bridge (AWB), it is preliminary disconnected from the BC and a dc constant voltage is applied to its *cd* diagonal. The balance is indicated at the diagonal *ab*. It is achieved at static armature conditions by varying the resistor R_{16}. At running conditions the emf E of the armature is proportional to the speed of rotation n. A voltage divider R_{18}, R_{19} is providing the proper level of the feedback voltage V_{fb}. At running conditions [5], [6] the current I_{ab} through R_{18} and R_{19} is proportional to E. Since $V_{fb} = R_{19}I_{ab}$, it follows that the feedback voltage V_{fb} is directly proportional to the speed n. V_{fb} is compared with the reference voltage V_r obtained from the voltage divider R_{12}, R_{13}. By varying the reference voltage, the driving torque T_D of the motor can be preliminary set to a given value. The comparator U1 is designed as a nonlinear element with saturation and it is realized by an operational amplifier connected in an open-loop configuration. It can be easily redesigned to operate as an ON-OFF element with hysteresis, for better performance of the system [6], [7], [8].

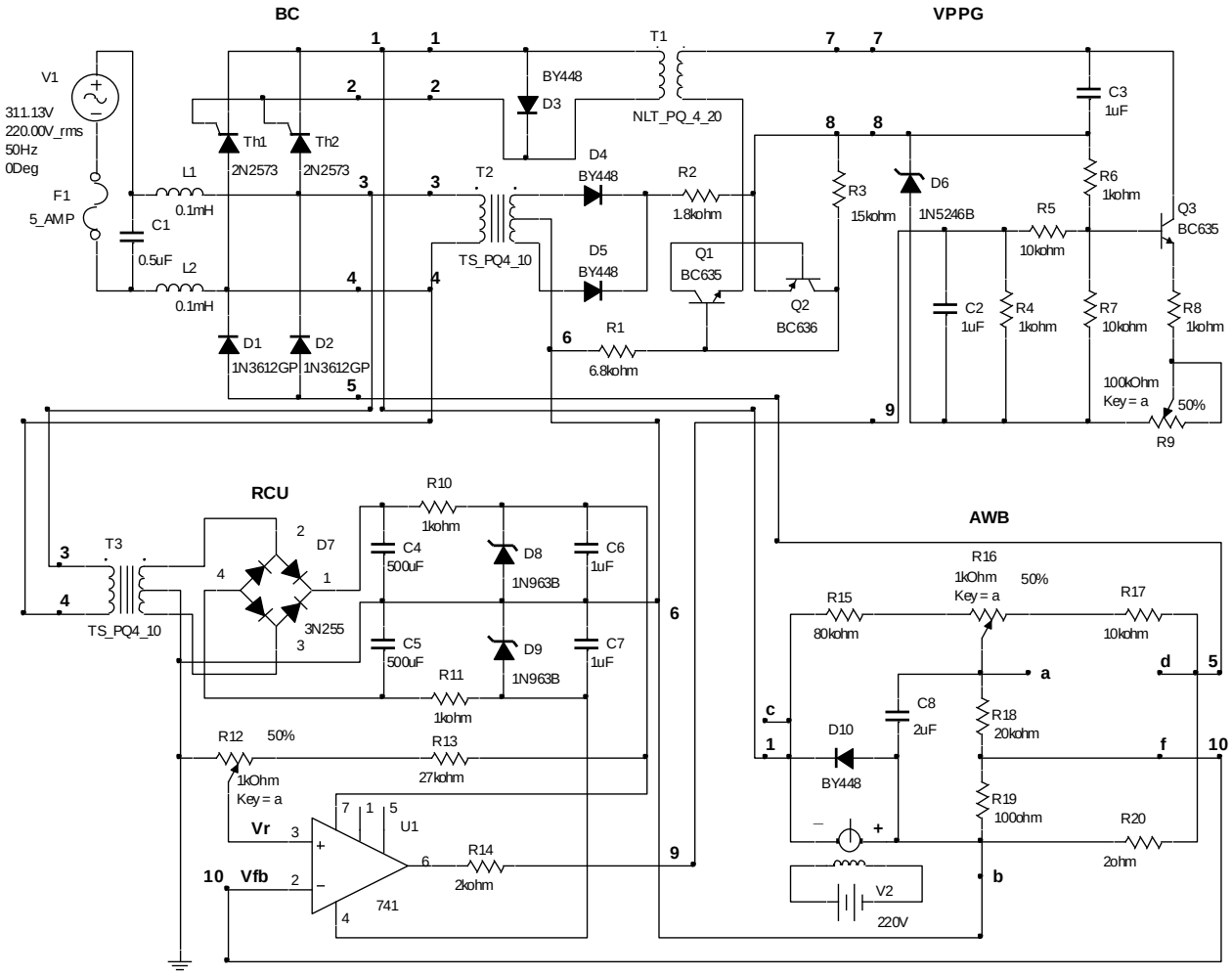

Figure 5: Electronic circuit diagram of the speed control system

During each half cycle of the line voltage the CG charges the capacitor C_3. The charging current is constant and the voltage V_c across C_3 increases linearly. At a preliminary selected value of this voltage the TU is activated.

The charging time of C_3 can be varied by the resistor R_9 controlling the thyristor firing angles α. In this way the speed of the motor can be selected and set accordingly by varying R_9.

The TU includes the transistors Q_1 and Q_2. During the charging of C_3 they are cut-off. When V_c reaches its critical value Q_1 and Q_2 saturate. C_3 discharges rapidly via the primary winding of the pulse transformer Tr_1. The thyristors Th_1 or Thr_2 are fired by a pulse developed at the secondary winding of Tr_1.

V. Stability Analysis of the Control System

The speed control system, described by the electronic circuit diagram, consists of a linear and a nonlinear section. The system's stability analysis can be performed by applying of the Goldfarb stability criterion, also known as the Describing Function analysis [7], [8]. The complete block diagram of the speed control system is shown in Figure 6.

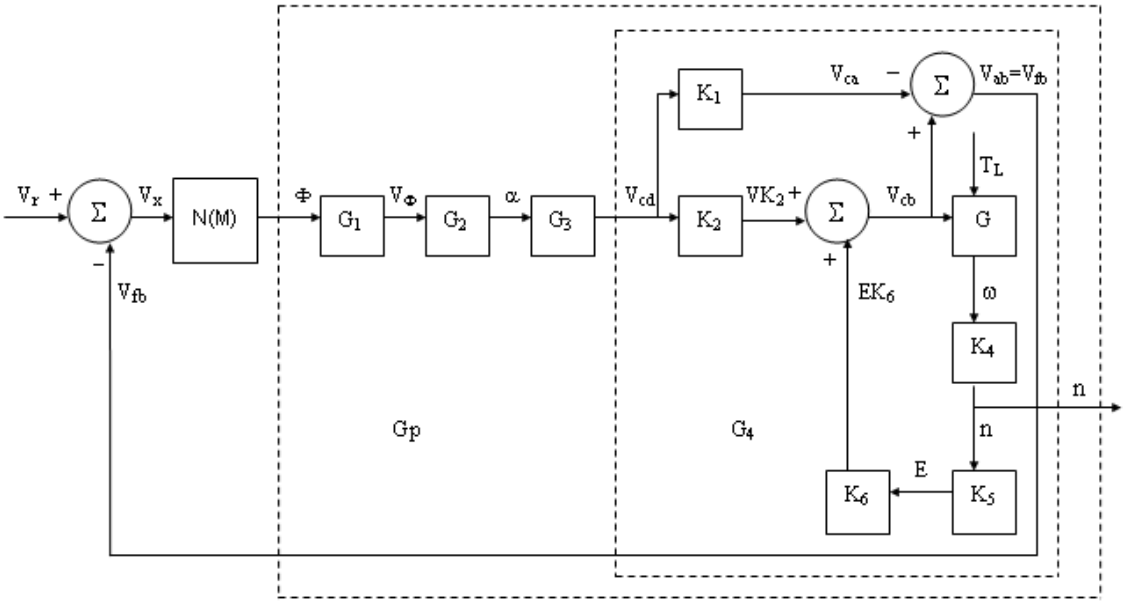

Figure 6: Block diagram of the speed control system

The block diagram of the speed control system can be simplified as shown in Figure 7.

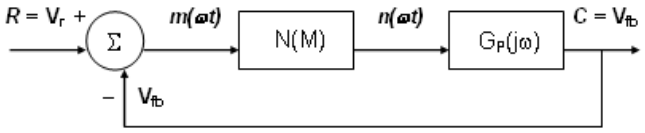

Figure 7: Modified block diagram of a closed-loop system

The Describing Function analysis assumes that the output of a nonlinear element is a periodic signal having the same fundamental frequency as that of the input where all harmonics and any dc component are neglected.

Following the conception of the describing function analysis [9], [10], the transfer function of the nonlinear element can be presented as:

$$N(M) = \frac{n(\omega t)}{m(\omega t)} \approx \frac{N_1 \sin(\omega t + \varphi_1)}{M \sin \omega t} \qquad (13)$$

Then, the transfer function of the closed-loop system shown in Figure 7.1 becomes:

$$\frac{C}{R} = \frac{N(M)G_P(j\omega)}{1 + N(M)G_P(j\omega)} \qquad (14)$$

Accordingly, the characteristic equation of the closed-loop system is [9], [10]:

$$1 + N(M)G_P(j\omega) = 0 \qquad (15)$$

or $$G_P(j\omega) = -\frac{1}{N(M)} = Z(M) \qquad (16)$$

The characteristic equation (15) is also known as the harmonic balance equation. The harmonic balance equation is a necessary condition for the existence of limit cycles in the nonlinear system [8], [9], [10]. The Describing Function analysis can be considered as a linear approximation of a static nonlinearity limited to the first harmonic [9], [10]. The accuracy of the analysis is even better for higher-order systems since they have better low-pass filter characteristics. The harmonic balance equation is similar to the characteristic polynomial function that leads to the Nyquist condition for closed-loop stability.

If equation (16) is satisfied, then the system output will be experiencing a limit cycle. This corresponds to the case where the $G_P(j\omega)$ locus passes through a critical point. While in the conventional frequency-response analysis of linear control systems, the critical point is (-1, j0), in the describing function analysis, the critical point is modified so that the entire $Z(M) = -1/N(M,\omega)$ locus becomes a locus of critical points. Therefore, the relative location and intersection of the $Z(M) = -1/N(M,\omega)$ locus and the $G_P(j\omega)$ locus will provide the stability information [9], [10].

The stability of a nonlinear system is determined by plotting the $Z(M) = -1/N(M,\omega)$ locus and the $G_P(j\omega)$ locus on a common plane. There is an important precondition that $G_P(j\omega)$ should correspond to a stable stand-alone system.

The constants and the dynamic properties of the different structural blocks are determined by considering the values of all the components and the parameters of the dc motor. Then, taking into account the variable gain K, the transfer function of the total linear section is revealed by the following expression [11], [12]:

$$G_P(s) = \frac{21600K}{0.0126s^3 + 1.98s^2 + 72s + 1000} \qquad (17)$$

The nonlinear part of the control system is behaving as a nonlinear ON-OFF element with hysteresis. Its transfer function is:

$$N(M) = \frac{4K}{\pi M}\angle -\sin^{-1}\left(\frac{h}{M}\right) \qquad (18)$$

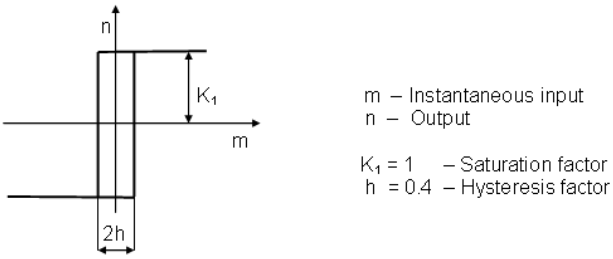

Figure 8: Characteristic and properties of the ON-OFF nonlinearity with hysteresis

where M is the amplitude of the input variations

It is assumed that the parameters of the nonlinearity (K_1 = 1 and h = 0.4) are constant. A function $Z(M)$ is obtained by applying equation (18). The results for different amplitudes M are shown in Table I.

TABLE I Z(M) = -1/N(M) AT DIFFERENT AMPLITUDES M

M	0.4	0.8	1.6	2.4
N(M)	3.18∠–90°	1.59∠–30°	0.8∠–14°	0.53∠–10°
Z(M)	–0.31∠+90°	–0.63∠+30°	–1.25∠+14°	–1.9∠+10°

To determine the stability margins of $G_P(j\omega)$ as a stand-alone system, the D-Partitioning analysis is applied in the discrete-time domain with the aid of the bilinear transform. By implementing the Euler's approximation, the sampling period T_s should be within the range $T_s \le (0.1T_{min}$ to $0.2T_{min})$, where T_{min} is the minimum time-constant of the continuous-time system or the analogue plant model prototype [13], [14], [15]. From the characteristic equation of the continuous independent plant $G_P(s)$:

$$G(s) = 0.0126s^3 + 1.98s^2 + \\ + 72s + 1000 + 21600K = 0 \qquad (19)$$

The variable parameter K of the linear section of the system is determined as:

$$K(s) = -\frac{0.0126s^3 + 1.98s^2 + 72s + 1000}{21600} \qquad (20)$$

Initially, the variable $K(s)$ is introduced as a continuous function. To provide the opportunity for a potential introduction of a digital controller, next it is converted into its digital equivalent $K(z)$ with the aid of the bilinear transform [16]. The D-Partitioning is achieved in the discrete-time domain in terms of the variable gain K as follows:

```
>> K=tf([-0.0126 -1.98 -72 -1000],[0 21600])
Transfer function:
-0.0126 s^3 - 1.98 s^2 - 72 s - 1000
-----------------------------------
          21600
>> Kd1 = c2d(K,0.001,'tustin')
Transfer function:
-5040 z^3 + 1.436e004 z^2 - 1.363e004 z + 4307
-----------------------------------------------
        z^3 + 3 z^2 + 3 z + 1
Sampling time: 0.001
>> dpartition(Kd1)
```

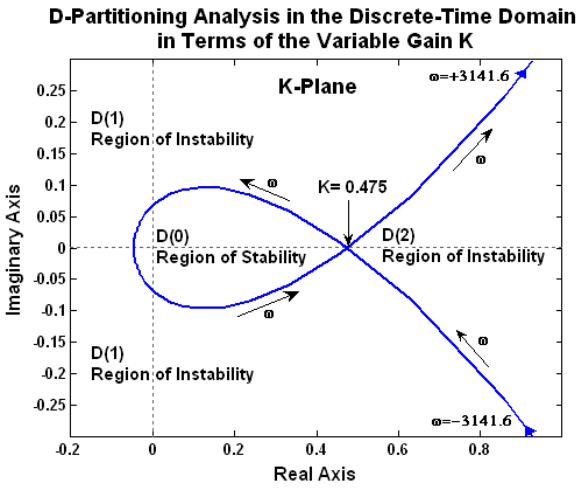

Figure 9: D-Partitioning analysis in the discrete-time domain of the linear section prototype in terms of the variable gain K

The D-Partitioning curve, plotted in the *K*-plane and as seen in Figure 9, is considered within the frequency range $\omega = \pm \omega_s/2 = \pm 2\pi/2T_s = \pm 3141.6$ rad/sec [17].

The D-Partitioning determines three regions on the *K*-plane: D(0), D(1) and D(2). Only D(0) is the region of stability, being always on the left-hand side of the curve [17], [18], [19]. Therefore, $G_P(j\omega)$ will be stable only when $0 \le K \le 0.475$. The performance of the entire system depends on the stability of the continuous linear section as a stand alone system. Further, $Z(M) = -1/N(M,\omega)$ locus and the $G_P(j\omega)$ locus at (K = 0.1, 0.25 and 0.4) are plotted on a common plane as shown in Figure 10. This is achieved by applying the following code:

```
>> Gp01=tf([0 2160],[0.0126 1.98 72 1000])
Transfer function:
        2160
-----------------------------------
0.0126 s^3 + 1.98 s^2 + 72 s + 1000
>> Gp025=tf([0 5400],[0.0126 1.98 72 1000])
Transfer function:
        5400
-----------------------------------
0.0126 s^3 + 1.98 s^2 + 72 s + 1000
>> Gp04=tf([0 8640],[0.0126 1.98 72 1000])
Transfer function:
        8640
-----------------------------------
0.0126 s^3 + 1.98 s^2 + 72 s + 1000
>> Gp1d=c2d(Gp01,0.001,'tustin')
Transfer function:
  1.984e-005 z^3 + 5.952e-005 z^2 + 5.952e-005 z + 1.984e-005
-------------------------------------------------------------
      z^3 - 2.849 z^2 + 2.704 z - 0.8545
Sampling time: 0.001
>> Gp2d=c2d(Gp025,0.001,'tustin')
Transfer function:
4.96e-005 z^3 + 0.0001488 z^2 + 0.0001488 z + 4.96e-005
-------------------------------------------------------
      z^3 - 2.849 z^2 + 2.704 z - 0.8545
Sampling time: 0.001
>> Gp3d=c2d(Gp04,0.001,'tustin')
Transfer function:
7.936e-005 z^3 + 0.0002381 z^2 + 0.0002381 z + 7.936e-005
---------------------------------------------------------
    z^3 - 2.849 z^2 + 2.704 z - 0.8545
Sampling time: 0.001
>> nyquist(Gp1d,Gp2d,Gp3d)
```

According to the Goldfarb stability criterion, the control system is stable for any one of the cases, since each locus G_{P1d}, G_{P2d} or G_{P3d} is not enclosing the point (-1, j0) of the complex plane and also is not enclosing this part of the characteristic $Z(M)$, corresponding to the increment of M after a crossing point (M,ω), related to a limit cycle [7], [20], [21], [22].

Due to the variation of the linear section gain K, the limit cycles are with different amplitude M and frequency of oscillation ω as seen from Figure 10.

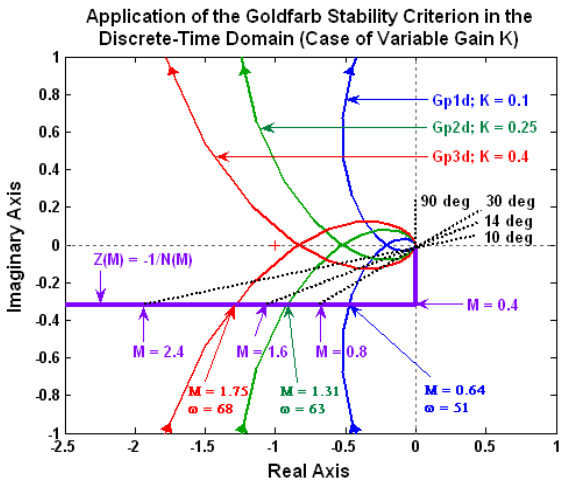

Figure 10: Application of the Goldfarb stability criterion

VI. Load Characteristics of the DC Motor Incorporated into Control System

Comparison of the load steady-state characteristics of the dc motor $n = f(T)$, before and after application of the feedback control, is shown in Figure 11. At a load torque T_L = 0.6Nm and V_{bc} = 180V the relative drop in the motor's speed for the case of the open-loop system is 7.78%, while for the closed-loop system it is only 1.11%. At T_L = 0.6Nm and V_{bc} = 50V the relative drop in speed is 22.8% without a feedback and 0.23% with a feedback.

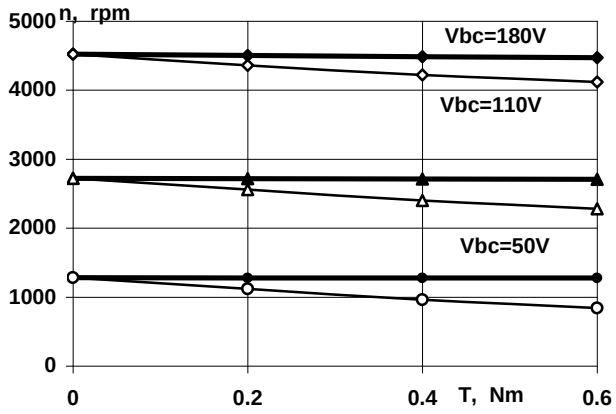

Figure 11: Load characteristics of the DC motor with and without a feedback

VII. Conclusions

A tight speed control system of a dc motor drive is suggested and analyzed. The armature circuit of a dc motor is connected as one of the ratio arms of a Wheatstone bridge, now becoming an active dc bridge (ADCB). This is a unique solution for accurate control of a dc motor speed, since armature emf E, induced at running conditions of the dc motor can be used as a precise feedback signal. Analyzing the ADCB, it was proven that the bridge output voltage $V_{ab} = V_{fb}$ depends directly on the induced armature emf E and hence on the motor speed n.

The suggested type of the nonlinear stage used in the system is an ON-OFF element with hysteresis. The control system is analyzed for stability with the aid of the Goldfarb stability criterion. As a stability precondition, it is proven that if the gain factor K is within the range $0 \leq K \leq 0.475$, the continuous linear section as a stand alone system will be stable. Also it is proven that the complete control system is stable since the locus the continuous linear section, for $0 \leq K \leq 0.475$, is not enclosing this part of the characteristic $Z(M)$, corresponding to the increment of M after a crossing point (M,ω), related to a limit cycle.

The developed control system operates in a limit cycle at specific magnitude M and frequency of oscillation ω, which occurs due to the continuous comparison between feedback voltage V_{fb} and the reference voltage V_r. This is a typical mode of operation for some industrial control systems containing nonlinear elements.

The advantages of the suggested speed control system can be seen in the best way from the load steady-state characteristics of the dc motor. They show almost constant motor's speed for a specified range of the load torque. The developed tight-speed control system is tested successfully in laboratory conditions. It can be implemented in a variety of industrial motor drive applications, subjected to variable load, where constant speed is required.

REFERENCES

[1] Shinners J. S., Modern Control System Theory, 3rd ed., New York: McGraw-Hill, pp.190-203, 2004.

[2] Ogata, K, Modern Control Engineering, Prentice-Hall International Editions Inc., pp. 48-52, 2006.

[3] Kuo B.C., Automatic control systems, New York, USA, McGraw-Hill, pp.521-530, 2010.

[4] Gray B., Electrical Machines and Drive Systems, ELBS, Longman Group UK Ltd., pp. 446, 2007.

[5] Graf R. F., Encyclopedia of Electronic Circuits, TAB Books, Blue Ridge Summit, PA, McGraw-Hill, Inc., USA, pp. 838, 2001.

[6] Savant C. J., M. S. Roden, G.L. Carpenter, Electronic Design - Circuits and Systems, The Benjamin/ Cummings Publishing Company, Inc., Redwood, California, USA, pp. 831, 2007.

[7] Netushila A. V., L. S. Goldpharb, G. K., Control System Theory, Vishaia Shkola Publishing Company, Moscow, USSR, pp. 424, 2007.

[8] Naumov, N., Nonlinear Feedback Control Theory, Nauka Publishing Company, Moscow, pp. 487-521, 2006.

[9] Atherton D. P., Nonlinear Control Engineering – Describing Function Analysis and Design, Van Nostrand Reinhold Company, New York, pp. 113-237, 2005.

[10] Shinners S.M., Modern Control System Theory, Addison-Wesley Publishing Company, pp.369-472, 2004.

[11] Yanev K.M, Anderson G.O., Masupe S., Stability and Robustness of a Control System for Precise Speed Control, International Journal of Energy Systems, Computers and Control, Volume 2, No. 1, ISSN: 0976-6782, pp. 11–24, 2011.

[12] Yanev K.M., Advanced Interactive Tools for Analysis and Design of Nonlinear Robust Control Systems, International Review of Automatic Control, ISSN: 1974-6059, Vol. 6, N. 6, pp. 720-727, 2013.

[13] Euler Method, In Wikipedia. Retrieved March 27, 2014, http://en.wikipedia.org/wiki/Euler_method

[14] Discrete Systems.Retrieved October 17, 2014, http://www.eng.ox.ac.uk/~conmrc/dcs/dcs1.pdf

[15] Continuous-Discrete Conversion Methods. MathWorks R2014b Documentation, Retrieved October 17, 2014, http://www.mathworks.com/help/control/ug/continuous-discrete-conversion-methods.html#bs78nig-1

[16] Tustin with Frequency Prewarping. MathWorks R2014b Documentation. Retrieved October 17, 2014, http://radio.feld.cvut.cz/matlab/toolbox/control/manipmod/ltiops20.html

[17] Yanev K. M., Application of the Method of D-Partitioning for Stability of Control Systems with Variable Parameters, BJT, Vol.16, Number 1, pp.51-58, 2007.

[18] Neimark Y., D-partition and robust stability, Computational Mathematics and Modeling, 9(2), pp. 160-166, 2006.

[19] Yanev K.M., *Advanced D-Partitioning Stability Analysis in the 3-Dimensional Parameter Space,* International Review of Automatic Control, ISSN: 1974-6059, Vol. 6, N. 3, pp. 236-240, 2013.

[20] Yanev K.M, Strategy for Analysis and Design of a Digital Robust Controller for Nonlinear Control Systems, 4th IASTED Africa Conference on Modeling and Simulation, Gaborone, ISBN 978-0-88986-929-5, pp. 213-220, 2012.

[21] Yanev K.M., Advanced Interactive Tools for Analysis and Design of Nonlinear Robust Control Systems, International Review of Automatic Control, ISSN: 1974-6059, Vol. 6, N. 6, pp. 720-727, 2013.

[22] Bhattacharyya S., The Parametric Approach, Englewood Cliffs, NJ, Prentice Hall, pp.325-387, 2005.